Supplementary Material for The normal stress dependence of rock friction

Sylvain Barbot * [1]

[1]Department of Earth Sciences, University of Southern California, Los Angeles, USA

*Corresponding author: sbarbot@usc.edu

Supplementary Tables

- Table S1. Best-fitting power-law parameters μ_0 and β for the constitutive friction law of Equation (1) with $\sigma_0 = 1$ MPa. The uncertainty is indicated by the number of relevant digits.

Supplementary Figures

- Figure S1. Comparison of linear and power-law models for Darley Dale sandstone (*Murrell*, 1965).
- Figure S2. Comparison of linear and power-law models for Ormonde siltstone (*Barton*, 1973).
- Figure S3. Comparison of linear and power-law models for Bilsthorpe mudstone (*Barton*, 1973).
- Figure S4. Comparison of linear and power-law models for Hucknall shale (*Barton*, 1973).
- Figure S5. Comparison of linear and power-law models for phyllosilicate-rich gouge (*Hirauchi et al.*, 2020a).
- Figure S6. Comparison of linear and power-law models for powdered Pozzolanic mortar at 100% humidity at room temperature after holds of 3, 30, 300, 3,000, and 30,000 s for normal stress from 0.5 MPa to 80 Mpa (*Volpe et al.*, 2025, 2026).

Table S1 Best-fitting power-law parameters μ_0 and β for the constitutive friction law of Equation (1) with $\sigma_0 = 1$ MPa. The uncertainty is indicated by the number of relevant digits.

Reference	Material	μ_0	β	Reference	Material	μ_0	β
Barton (1973)	Ormonde siltstone	1.73	0.27	*Hoskins et al.* (1968)	Sandstone	0.75	0.18
	Bilsthorpe mudstone	1.73	0.31		Trachyte rough	1.07	0.25
	Hucknall shale	1.65	0.25		Trachyte 350 µm	1.01	0.29
	Bilsthorpe mudstone	1.10	0.19		Wombeyan marble	1.75	0.36
Barton (1976)	Weber sandstone A	1.38	0.12	*Ikari et al.* (2007)	30% Montmorillonite	0.72	0.11
	Weber sandstone B	1.71	0.15		50% Montmorillonite	1.10	0.34
	Weber sandstone C	0.94	0.04		70% Montmorillonite	0.74	0.34
Beeman et al. (1988)	Ice at 77 K	1.10	0.31		100% Montmorillonite	0.11	0.23
Bedford et al. (2021)	Nankai C0002 Pf= 5MPa	0.32	0.05	*Jaeger* (1959)	Plaster	0.92	0.08
	Nankai C0002 Pf=10MPa	0.53	0.05	*Jang and Jang* (2015)	Plaster (N2000)	0.73	0.08
	Nankai C0002 Pf=25MPa	0.54	0.09		Plaster (GM 10)	2.10	0.29
	Nankai C0002 Pf=50MPa	0.42	0.02		Plaster (Diestone)	1.12	0.09
	Nankai C0002 Pf=75MPa	0.43	0.01	*Kurzawski et al.* (2018)	Calcareous clay 14H6	0.09	-0.38
Byerlee (1968)	Westerly granite	1.69	0.13		Silt 42X4	0.11	-0.32
	Spruce Pine dunite	2.43	0.19		Silty clay 2H1	.001	-1.28
	Solenhofen sandstone	7.14	0.43		Clayey siltstone 8R6	0.02	-0.61
	Oak Hall limestone	2.93	0.22	*Lilly* (1982)	Shale	0.42	0.26
	Nahant gabbro	2.37	0.19	*Maegawa et al.* (2015)	PDMS 1	0.60	0.11
	Cabramurra serpent.	1.82	0.15		PDMS 2	0.45	0.13
Carpenter et al. (2009)	MHST1 siltstone	0.62	-0.01	*Maksimović* (1992)	Sandstone	1.21	0.21
	B2125 arkosic sandstone	0.67	0.04		Micaschist	0.86	0.29
	B18R4 arkosic sandstone	0.71	0.05	*Mehrishal et al.* (2016)	Onyx marble (1 mm/s)	0.13	0.14
	B1R1 granodiorite	0.65	0.02	*Mizukami and Maeno* (2000)	Ice slow	0.05	0.19
	Siliceous mudstone	0.72	0.04		Ice intermediate	.003	0.59
	Great Valley turbidite	0.69	0.03		Ice fast	0.01	0.41
	Monterey mudstone	0.59	-0.02	*Moore et al.* (2004)	Chrysotile 100°C	0.01	-0.72
	Temblor sandstone	0.60	-0.01		Chrysotile 194°C	0.02	-0.56
	New Idria serp. (dry)	0.29	0.09		Chrysotile 281°C	0.07	-0.40
	Etchegoin sandstone	0.62	-0.01	*Moore and Lockner* (2008)	Muscovite	0.23	-0.13
	Franciscan clay	0.61	-0.01		Montmorillonite	0.06	-0.25
	Varian Ranch formation	0.68	0.02		Talc	0.15	-0.06
	Serpentinite Chips	0.70	0.03		Biotite	0.15	-0.16
	Unconsol. gravel & sand	0.63	0.02	*Morrow and Byerlee* (1989)	Ottawa sand	0.98	0.07
Carpenter et al. (2016)	Calcite	0.66	0.01		Quartzite	0.90	0.06
Chang et al. (2024)	Halite	0.33	0.17		Westerly granite	1.19	0.16
Coulomb (1821)	Oak-pine contact	0.59	0.04	*Morrow et al.* (2017)	Wet montmorillonite	0.04	-0.28
	Oak wood 2	0.28	-0.01	*Mutlu and Bobet* (2006)	Gypsum	0.44	0.03
	Oak (kinetic)	0.09	0.06	*Saffer and Marone* (2003)	Quartz	0.83	0.07
	Oak wood	0.52	-0.03		Illite shale	0.82	0.14
	Pine wood	0.60	-0.02		50% smectite	1.17	0.37
	Elm wood	0.45	0.00		Smectite	1.17	0.54
Giorgetti et al. (2015)	5% talc	0.62	0.06	*Sakuma et al.* (2018)	Dry mica	0.34	0.10
	20% talc	0.31	-0.04	*Schellart* (2000)	Caster sugar	0.24	0.26
González et al. (2024)	SCF01	0.72	0.18		Sand S1	0.17	0.27
	CCF11	0.73	0.30		Sand S2	0.16	0.28
	CCF13	0.75	0.25		GM1	0.65	0.07
	CHF09	0.53	0.09		GM2	0.22	0.19
	MF14	0.52	0.04	*Schulson and Fortt* (2012)	Ice 263 K	0.13	0.47
	MF15	0.66	0.27	*Smith and Faulkner* (2010)	L5 dry	0.18	-0.31
	PPF10	0.39	0.02		L5 wet	0.14	-0.30
	PPF12	0.40	0.05		L4 cataclasite	0.23	-0.27
Handin (1969)	Blair dolomite	1.07	0.16		L3.3 chlorite	0.26	-0.13
	Solenhofen limestone	1.06	0.10		L3.2 talc	0.21	-0.07
	Know dolomite	1.14	0.15		L2 schist	0.46	-0.10
	Tennessee limestone	0.97	0.06	*Smith et al.* (2017)	Green cataclasites	0.52	0.19
Hirauchi et al. (2020a)	Tremolite schist	0.17	-0.18		Black cataclasites	0.98	0.35
	Argillite	0.17	-0.23	*Tesei et al.* (2018)	Chrysotile	0.25	0.10
	Cataclasite	0.22	-0.07		Lizardite	0.39	0.15
	Talc schist	0.04	-0.28		Retrograde serpent.	0.42	0.07
	Serpentinite	0.82	0.09		Antigorite	0.83	0.10
Hirauchi et al. (2020b)	Halite	0.99	0.14	*Volpe et al.* (2025)	Pozzolanic mortar	0.93	0.08
				Yashima et al. (2015)	Glass	0.14	0.26

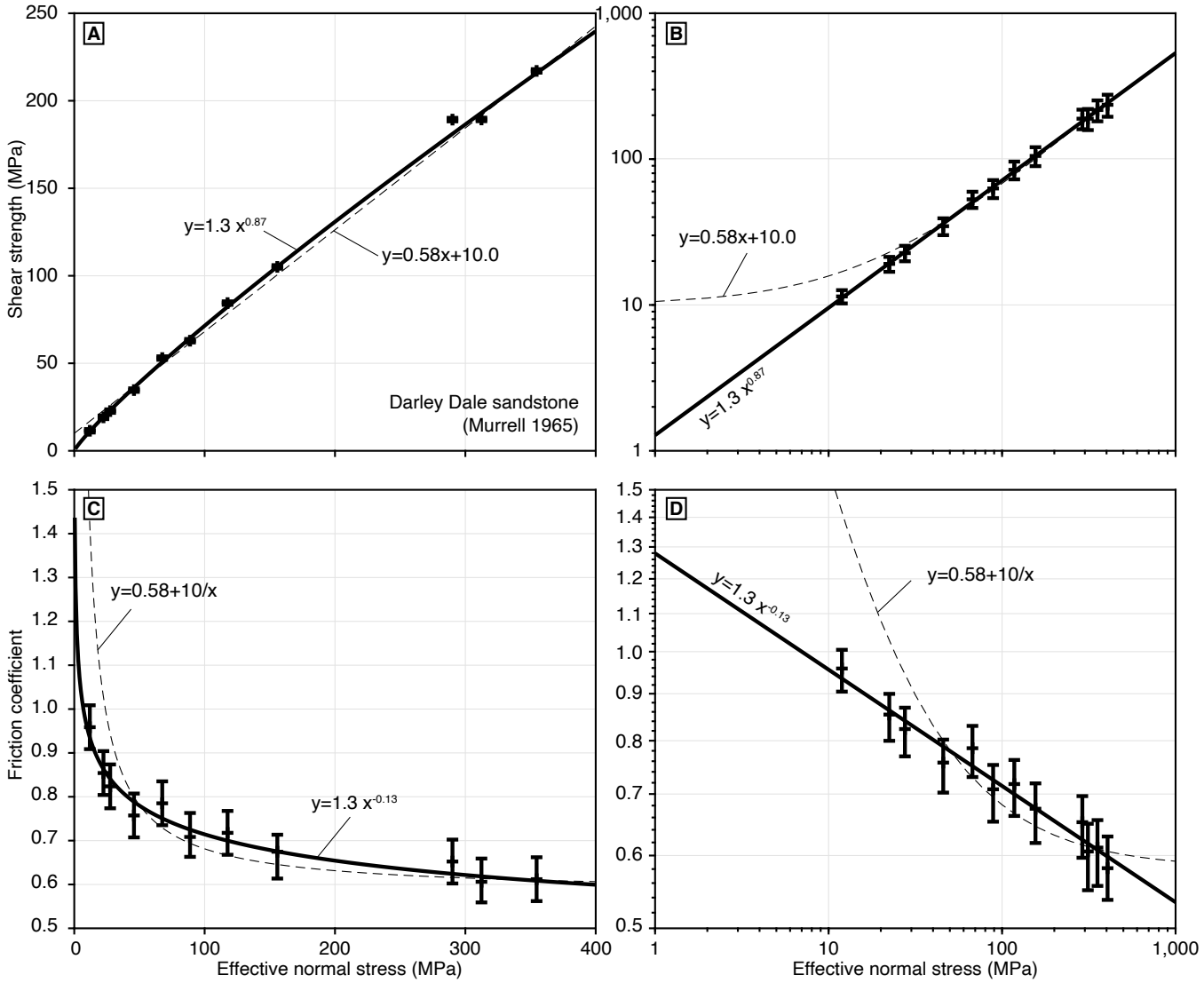

Figure S1 Comparison of linear and power-law models for Darley Dale sandstone (*Murrell*, 1965). A) Frictional strength of Darley Dale sandstone and corresponding linear (dashed lines) and power-law (solid lines) models with the best-fitting parameters indicated in the figure. B) Same in log-log plot, emphasizing the systematic residuals of the linear model at low normal stress. C, D) Friction coefficient in linear and log-log plots, respectively. The power-law model explains data satisfactorily, and does not feature systematic residuals.

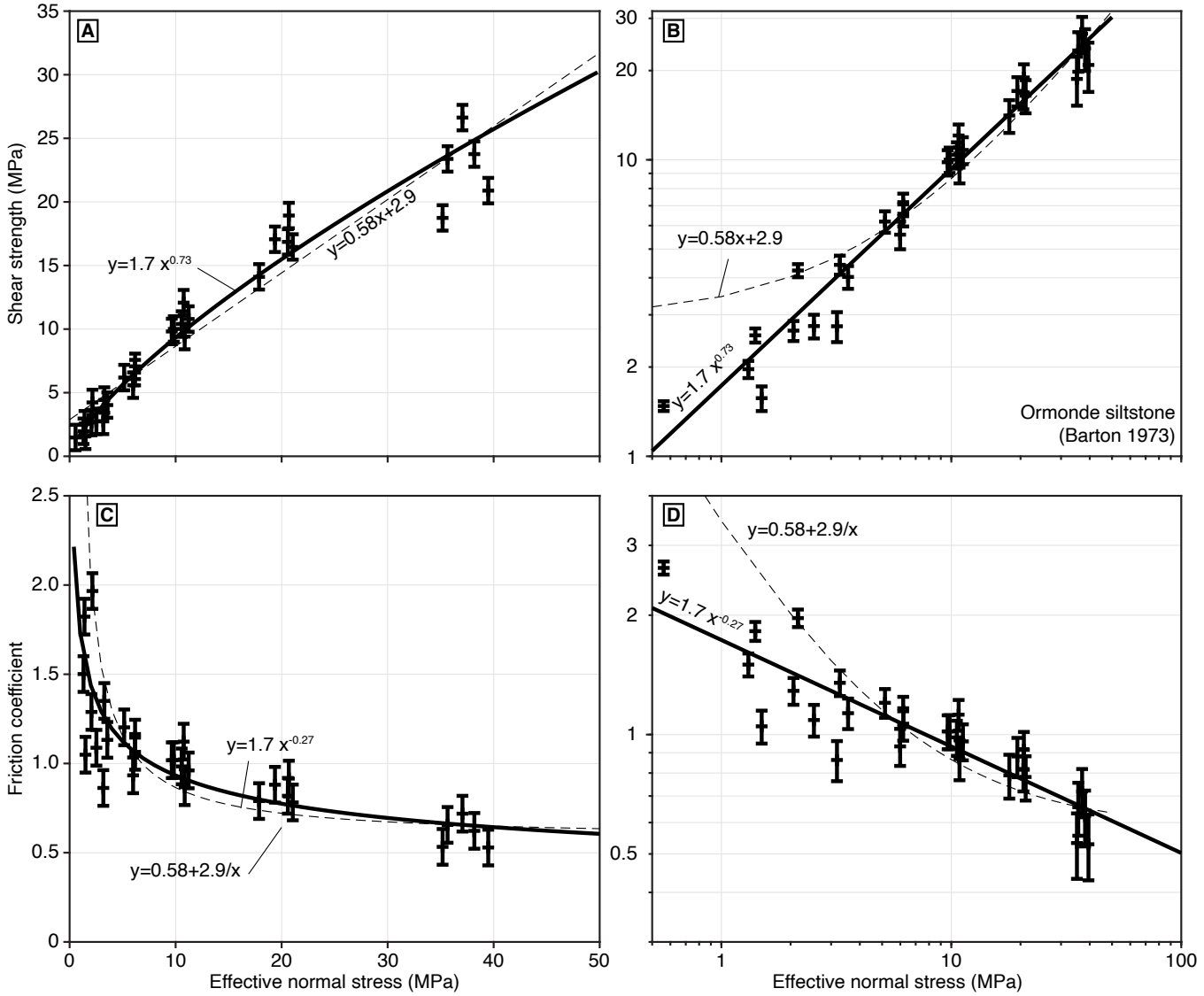

Figure S2 Comparison of linear and power-law models for Ormonde siltstone (*Barton*, 1973). A) Frictional strength of siltstone and corresponding linear (dashed lines) and power-law (solid lines) models with the best-fitting parameters indicated in the figure. B) Same in log-log plot, emphasizing the systematic residuals of the linear model at low normal stress. C, D) Friction coefficient in linear and log-log plots, respectively. The power-law model explains data satisfactorily, and does not feature systematic residuals.

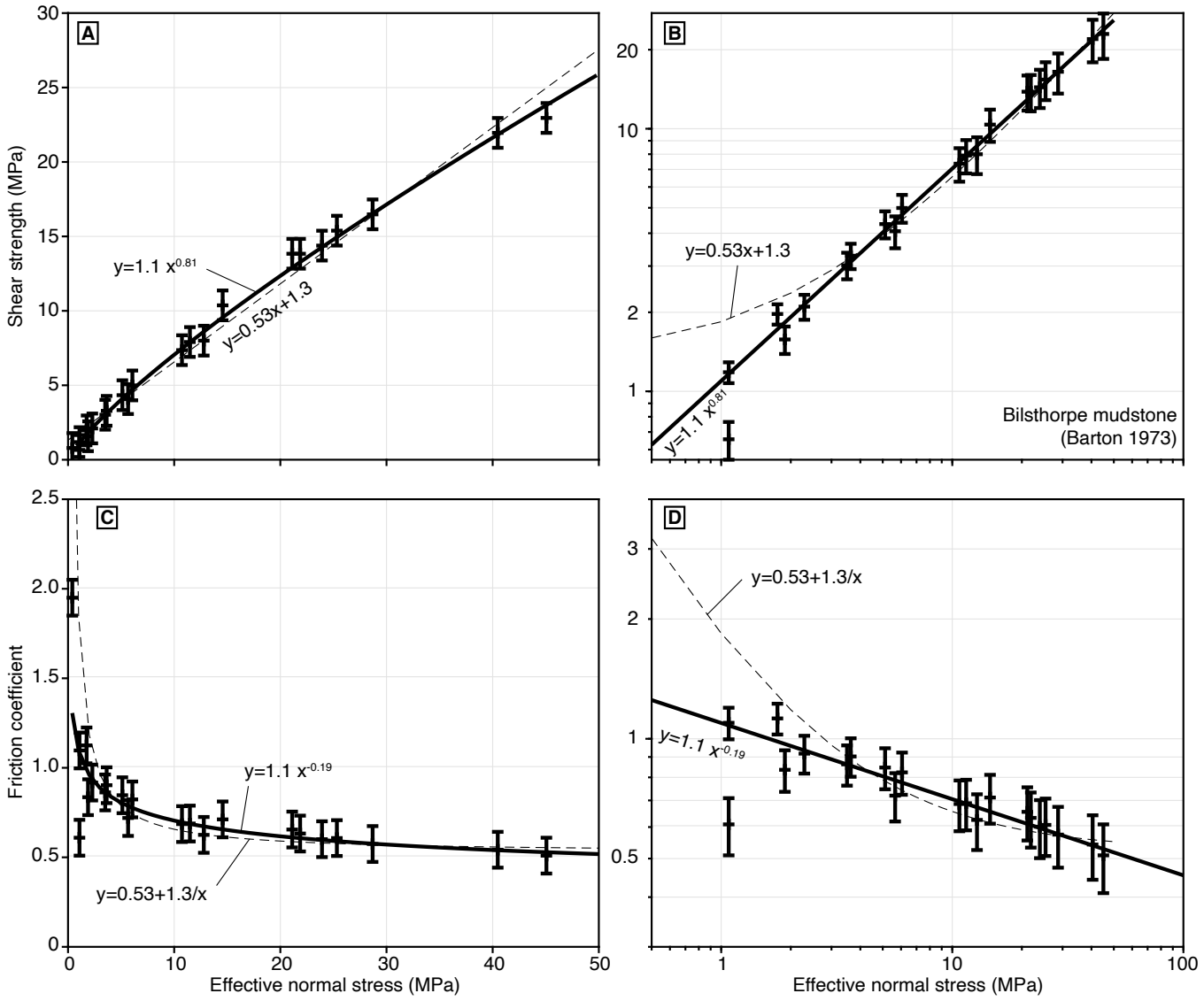

Figure S3 Comparison of linear and power-law models for Bilsthorpe mudstone (*Barton*, 1973). A) Frictional strength of mudstone and corresponding linear (dashed lines) and power-law (solid lines) models with the best-fitting parameters indicated in the figure. B) Same in log-log plot, emphasizing the systematic residuals of the linear model at low normal stress. C, D) Friction coefficient in linear and log-log plots, respectively. The power-law model explains data satisfactorily, and does not feature systematic residuals.

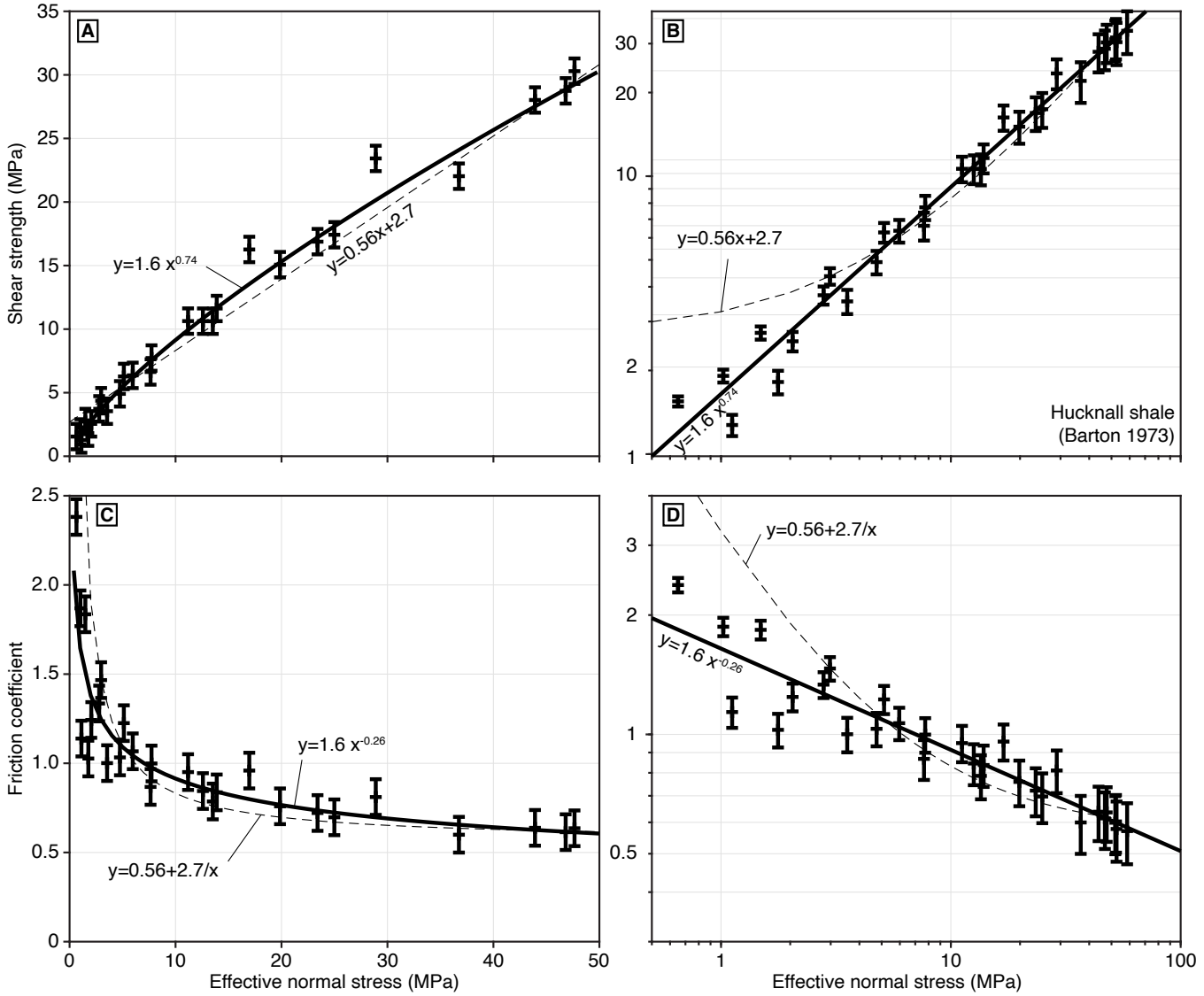

Figure S4 Comparison of linear and power-law models for Hucknall shale (*Barton*, 1973). A) Frictional strength of shale and corresponding linear (dashed lines) and power-law (solid lines) models with the best-fitting parameters indicated in the figure. B) Same in log-log plot, emphasizing the systematic residuals of the linear model at low normal stress. C, D) Friction coefficient in linear and log-log plots, respectively. The power-law model explains data satisfactorily, and does not feature systematic residuals.

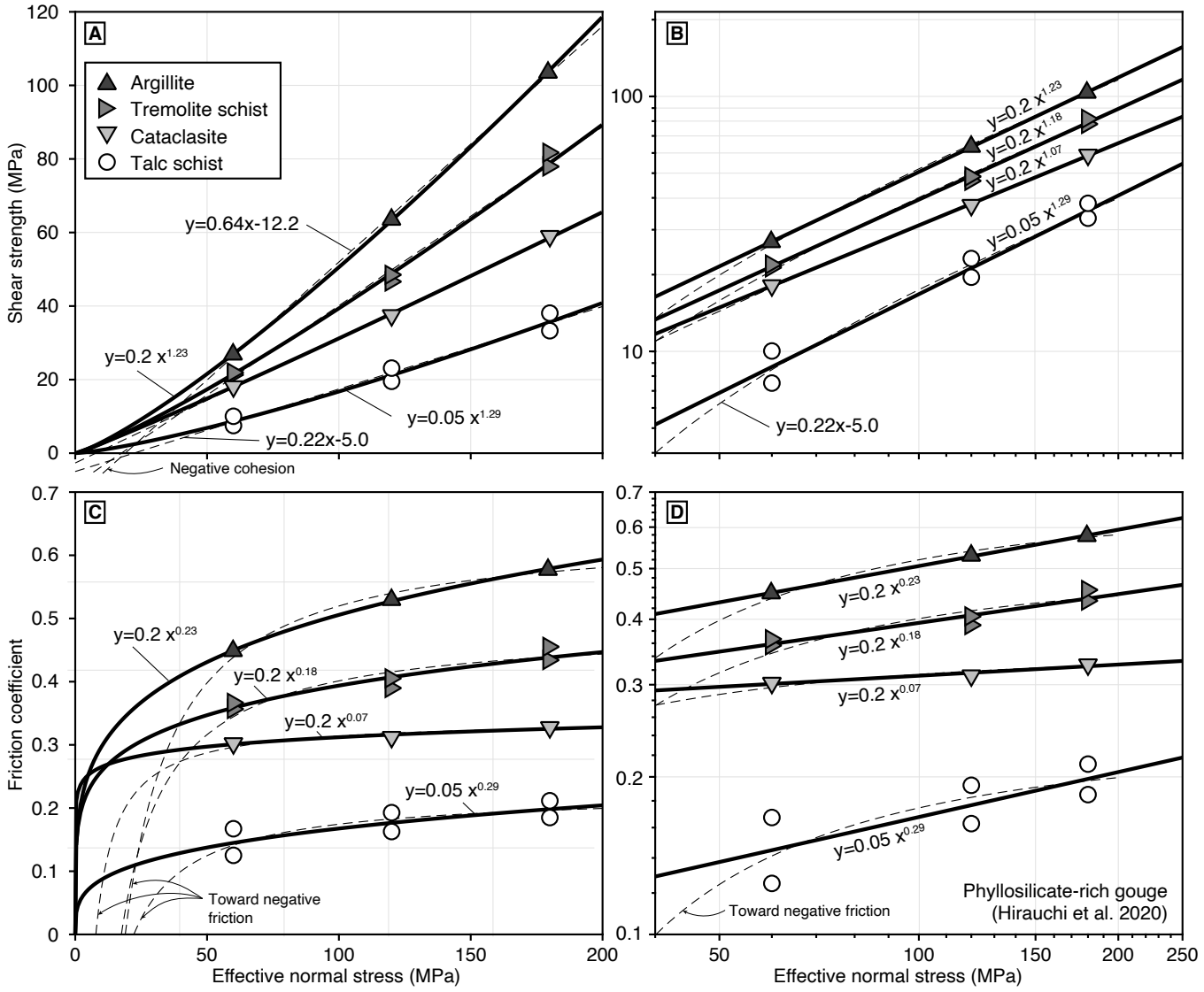

Figure S5 Comparison of linear and power-law models for phyllosilicate-rich gouge (*Hirauchi et al.*, 2020a). A) Frictional strength of argillite (dark upright triangle), tremolite schist (grey right triangle), cataclasite (grey downward triangle), and talc schist (circle) and corresponding linear (dashed lines) and power-law (solid lines) normal-stress dependence models. While the linear and power-law models explain the data equally well, all linear model predict negative intercept at the origin corresponding to negative strength for sufficiently low effective normal stress, an unphysical feature. B) Same as A for a log-log plot. C) Friction coefficient of argillite, tremolite schist, cataclasite, and talc schist and corresponding linear (dashed lines) and power-law (solid lines) models. The linear models all predict a negative friction coefficient for sufficiently low effective normal stress. The power-law models converge to zero at the origin. D) Same as C using a log-log plot. The results are representative of water-saturated phyllosilicate-rich gouge.

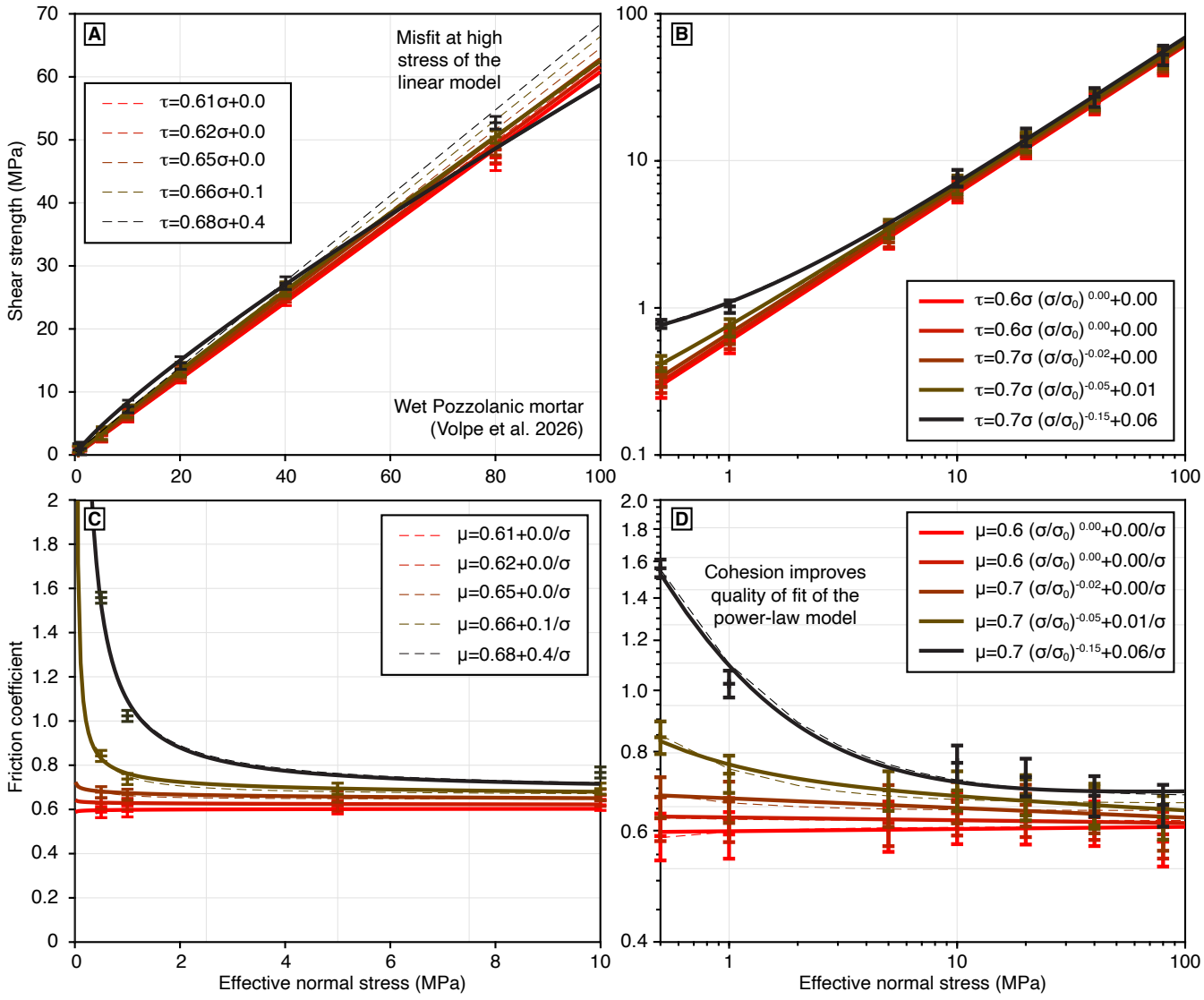

Figure S6 Comparison of linear and power-law models for powdered Pozzolanic mortar at 100% humidity at room temperature after holds of 3, 30, 300, 3,000, and 30,000 s for normal stress from 0.5 MPa to 80 Mpa (*Volpe et al.*, 2025, 2026). A) Comparison of the linear model of the form $\tau = c_0 + \mu_0\bar{\sigma}$ and a modified power-law model of the form $\tau = c_0 + \mu_0\sigma(\sigma/\sigma_0)^{-\beta}$. After holds of 3, 30, and 300 s, the linear model cannot simultaneously capture the low pressure and high pressure data. B) Same data and models shown in log-log plot. C) Comparison of the linear and power-law models at low stress, showing similar quality of fit of the linear and power-law models with cohesion. D) Same in a log-log plot. The power-law model requires a small cohesion terms of 10 kPa and 60 kPa for hold times of 3,000 and 30,000 s, respectively, to explain the frictional resistance at all pressure conditions. When considering data above 10 MPa normal stress, cohesion is not needed (*Barbot*, 2026).

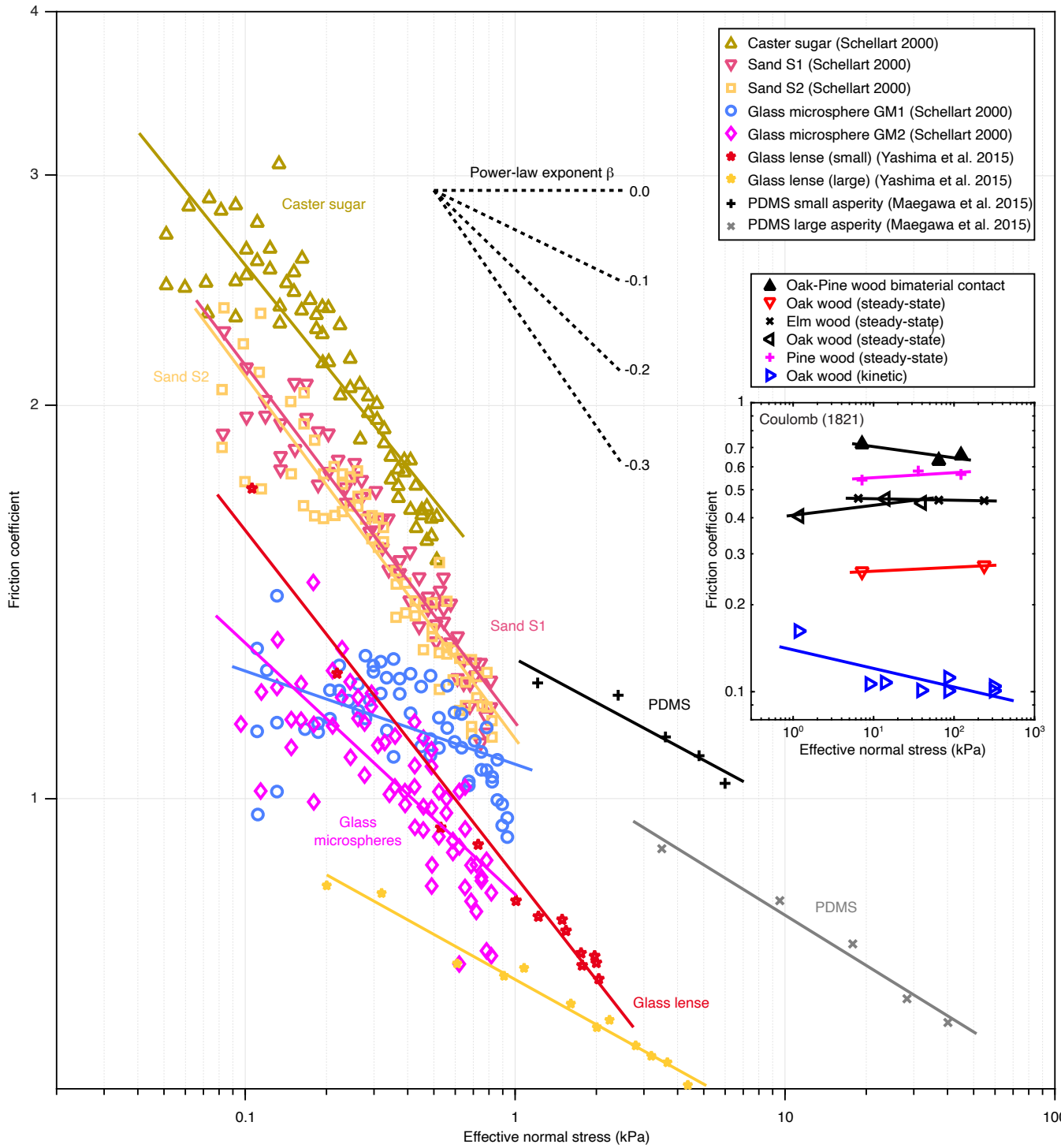

Figure S7 Friction coefficient of engineered surfaces and synthetic materials (*Coulomb*, 1821; *Schellart*, 2000; *Maegawa et al.*, 2015; *Yashima et al.*, 2015). The solid lines correspond to the best-fitting power-law relationship following Equation (1). The power-law exponents fall within $\beta = 0.17 \pm 0.08$ for those materials. The inset shows the low friction coefficient of oak, pine, and elm wood after a long healing phase (steady-state) and during high-velocity sliding (kinetic) (*Coulomb*, 1821).

References

Barbot, S., Comment on “the influence of cementation on fault stability", *Earth Planet. Sci. Lett.*, *678*, 119,845, doi: 10.1016/j.epsl.2026.119845, 2026.

Barton, N., Review of a new shear-strength criterion for rock joints, *Engineering geology*, *7*(4), 287–332, doi: 10.1016/0013-7952(73)90013-6, 1973.

Barton, N., The shear strength of rock and rock joints, in *International Journal of rock mechanics and mining sciences & Geomechanics abstracts*, vol. 13, pp. 255–279, Elsevier, doi: 10.1016/0148-9062(76)90003-6, 1976.

Bedford, J. D., D. R. Faulkner, M. J. Allen, and T. Hirose, The stabilizing effect of high pore-fluid pressure along subduction megathrust faults: Evidence from friction experiments on accretionary sediments from the Nankai Trough, *Earth Planet. Sci. Lett.*, *574*, 117,161, doi: 10.1016/j.epsl.2021.117161, 2021.

Beeman, M., W. Durham, and S. H. Kirby, Friction of ice, *J. Geophys. Res.*, *93*(B7), 7625–7633, doi: 10.1029/JB093iB07p07625, 1988.

Byerlee, J. D., Brittle-ductile transition in rocks, *J. Geophys. Res.*, *73*(14), 4741–4750, doi: 10.1029/JB073i014p04741, 1968.

Carpenter, B., C. Marone, and D. Saffer, Frictional behavior of materials in the 3d safod volume, *Geophys. Res. Lett.*, *36*(5), doi: 10.1029/2008GL036660, 2009.

Carpenter, B., C. Collettini, C. Viti, and A. Cavallo, The influence of normal stress and sliding velocity on the frictional behaviour of calcite at room temperature: insights from laboratory experiments and microstructural observations, *Geophys. J. Int.*, *205*(1), 548–561, doi: 10.1093/gji/ggw038, 2016.

Chang, C., H. Noda, Y. Hamada, C. Huang, T. Ma, G. Wang, and T. Yamaguchi, Comminution-induced transient frictional behavior in sheared granular halite, *Geophys. Res. Lett.*, *51*(21), e2024GL109,645, doi: 10.1029/2024GL109645, 2024.

Coulomb, C. A., *Théorie des machines simples, en ayant égard au frottement de leurs parties et à la roideur des cordages.*, Bachelier, 1821.

Giorgetti, C., B. Carpenter, and C. Collettini, Frictional behavior of talc-calcite mixtures, *J. Geophys. Res.*, *120*(9), 6614–6633, doi: 10.1002/2015JB011970, 2015.

González, Y., G. González, E. Spagnuolo, G. Pozzi, E. Jensen, S. Aretusini, and A. M. Schleicher, Exploring frictional properties of upper plate fault reactivation in subduction zones: The atacama fault system in northern chile, *Earth Planet. Sci. Lett.*, *648*, 119,106, doi: 10.1016/j.epsl.2024.119106, 2024.

Handin, J., On the coulomb-mohr failure criterion, *J. Geophys. Res.*, *74*(22), 5343–5348, doi: 10.1029/JB074i022p05343, 1969.

Hirauchi, K.-i., Y. Yamamoto, S. A. den Hartog, and A. R. Niemeijer, The role of metasomatic alteration on frictional properties of subduction thrusts: An example from a serpentinite body in the Franciscan Complex, California, *Earth Planet. Sci. Lett.*, *531*, 115,967, doi: 10.1016/j.epsl.2019.115967, 2020a.

Hirauchi, K.-i., Y. Yoshida, Y. Yabe, and J. Muto, Slow stick-slip failure in halite gouge caused by brittle-plastic fault heterogeneity, *Geochemistry, Geophysics, Geosystems*, *21*(9), e2020GC009,165, doi: 10.1029/2020GC009165, 2020b.

Hoskins, E., J. Jaeger, and K. Rosengren, A medium-scale direct friction experiment, in *International Journal of Rock Mechanics and Mining Sciences & Geomechanics Abstracts*, vol. 5, pp. 143–152, Elsevier, doi: 10.1016/0148-9062(68)90030-2, 1968.

Ikari, M. J., D. M. Saffer, and C. Marone, Effect of hydration state on the frictional properties of montmorillonite-based fault gouge, *J. Geophys. Res.*, *112*(B6), doi: 10.1029/2006JB004748, 2007.

Jaeger, J., The frictional properties of joints in rock, *Geofisica pura e applicata*, *43*(1), 148–158, 1959.

Jang, H.-S., and B.-A. Jang, New method for shear strength determination of unfilled, unweathered rock joint, *Rock Mechanics and Rock Engineering*, *48*(4), 1515–1534, doi: 10.1007/s00603-014-0660-3, 2015.

Kurzawski, R. M., A. R. Niemeijer, M. Stipp, D. Charpentier, J. H. Behrmann, and C. J. Spiers, Frictional properties of subduction input sediments at an erosive convergent continental margin and related controls on décollement slip modes: The Costa Rica Seismogenesis Project, *J. Geophys. Res.*, *123*(10), 8385–8408, doi: 10.1029/2017JB015398, 2018.

Lilly, P., The shear behaviour of bedding planes in mt mcrae shale with implications for rock slope design, *Int. J. Rock Mech. & Mining & Geomechanics Abstracts*, *19*(4), doi: 10.1016/0148-9062(82)90891-9, 1982.

Maegawa, S., F. Itoigawa, and T. Nakamura, Effect of normal load on friction coefficient for sliding contact between rough rubber surface and rigid smooth plane, *Tribology international*, *92*, 335–343, 2015.

Maksimović, M., New description of the shear strength for rock joints, *Rock mechanics and rock engineering*, *25*(4), 275–284, doi: 10.1007/bf01041808, 1992.

Mehrishal, S., M. Sharifzadeh, K. Shahriar, and J.-J. Song, An experimental study on normal stress and shear rate dependency of basic friction coefficient in dry and wet limestone joints, *Rock Mechanics and Rock Engineering*, *49*(12), 4607–4629, doi: 10.1007/s00603-016-1073-2, 2016.

Mizukami, N., and N. Maeno, Normal stress dependence of ice-ice friction coefficients, *Journal of the Japanese Society of Snow and Ice*, *62*(6), 515–521, doi: 10.5331/seppyo.62.515, 2000.

Moore, D. E., and D. A. Lockner, Talc friction in the temperature range 25°-400°C: Relevance for fault-zone weakening, *Tectonophysics*, *449*(1-4), 120–132, doi: 10.1016/j.tecto.2007.11.039, 2008.

Moore, D. E., D. A. Lockner, H. Tanaka, and K. Iwata, The coefficient of friction of chrysotile gouge at seismogenic depths, *International Geology Review*, *46*(5), 385–398, doi: 10.2747/0020-6814.46.5.385, 2004.

Morrow, C. A., and J. D. Byerlee, Experimental studies of compaction and dilatancy during frictional sliding on faults containing gouge, *Journal of Structural Geology*, *11*(7), 815–825, doi: 10.1016/0191-8141(89)90100-4, 1989.

Morrow, C. A., D. E. Moore, and D. A. Lockner, Frictional strength of wet and dry montmorillonite, *Journal of Geophysical Research: Solid*

Earth, *122*(5), 3392–3409, doi: 10.1002/2016JB013658, 2017.

Murrell, S. A. F., The effect of triaxial stress systems on the strength of rocks at atmospheric temperatures, *Geophys. J. Int.*, *10*(3), 231–281, doi: 10.1111/j.1365-246X.1965.tb03155.x, 1965.

Mutlu, O., and A. Bobet, Slip propagation along frictional discontinuities, *International Journal of Rock Mechanics and Mining Sciences*, *43*(6), 860–876, doi: 10.1016/j.ijrmms.2005.11.012, 2006.

Saffer, D. M., and C. Marone, Comparison of smectite-and illite-rich gouge frictional properties: application to the updip limit of the seismogenic zone along subduction megathrusts, *Earth Planet. Sci. Lett.*, *215*(1-2), 219–235, doi: 10.1016/S0012-821X(03)00424-2, 2003.

Sakuma, H., K. Kawai, I. Katayama, and S. Suehara, What is the origin of macroscopic friction?, *Science advances*, *4*(12), eaav2268, doi: 10.1126/sciadv.aav2268, 2018.

Schellart, W., Shear test results for cohesion and friction coefficients for different granular materials: scaling implications for their usage in analogue modelling, *Tectonophysics*, *324*(1-2), 1–16, doi: 10.1016/S0040-1951(00)00111-6, 2000.

Schulson, E. M., and A. L. Fortt, Friction of ice on ice, *J. Geophys. Res.*, *117*(B12), doi: 10.1029/2012JB009219, 2012.

Smith, S., and D. Faulkner, Laboratory measurements of the frictional properties of the Zuccale low-angle normal fault, Elba Island, Italy, *J. Geophys. Res.*, *115*(B2), doi: 10.1029/2008JB006274, 2010.

Smith, S., T. Tesei, J. Scott, and C. Collettini, Reactivation of normal faults as high-angle reverse faults due to low frictional strength: Experimental data from the Moonlight Fault Zone, New Zealand, *Journal of Structural Geology*, *105*, 34–43, doi: 10.1016/j.jsg.2017.10.009, 2017.

Tesei, T., C. Harbord, N. De Paola, C. Collettini, and C. Viti, Friction of mineralogically controlled serpentinites and implications for fault weakness, *J. Geophys. Res.*, *123*(8), 6976–6991, doi: 10.1029/2018JB016058, 2018.

Volpe, G., R. Affinito, L. Calzolari, G. Pozzi, C. Marone, and C. Collettini, The influence of cementation on fault stability, *Earth Planet. Sci. Lett.*, *671*, 119,674, doi: 10.1016/j.epsl.2025.119674, 2025.

Volpe, G., R. Affinito, L. Calzolari, G. Pozzi, C. Marone, and C. Collettini, Reply to the comment on “the influence of cementation on fault stability”, *Earth Planet. Sci. Lett.*, *679*, 119,867, doi: 10.1016/j.epsl.2026.119867, 2026.

Yashima, S., V. Romero, E. Wandersman, C. Frétigny, M. Chaudhury, A. Chateauminois, and A. Prevost, Normal contact and friction of rubber with model randomly rough surfaces, *Soft Matter*, *11*(5), 871–881, doi: 10.1039/C4SM02346C, 2015.